JOURNAL OF APPLIED ELECTROCHEMISTRY 16 (1986) 189–195

Current levelling behaviour under pulse current electroplating conditions: the role of reaction pseudocapacitance

HAROLD E. HAGER

Department of Chemical Engineering, BF-10, University of Washington, Seattle, WA 98195, USA

Received 3 October 1984; revised 2 March 1985

Despite growing interest in pulse current electroplating, published theories have not evolved beyond treatments of simple, single-step reaction kinetics. This omission of multiple-step kinetics and associated reaction pseudocapacitance is responsible for the inability to interpret mechanistically several key pulse current electrodeposition process characteristics.

A complex kinetics charge transfer model is developed to describe the enhanced geometric control of deposit thickness achievable with judiciously chosen pulse current control conditions. This semiquantitative analysis demonstrates that deposit thickness 'levelling' is primarily the result of the strong potential dependence of the reaction pseudocapacitance, together with proper choices of pulse current control variables. For any system of interest, a well defined on-time current, I_A, and on-time and off-time periods, t_A and t_B, are optimum for minimizing relative deposit thickness variation.

1. Introduction

Metal electrodeposition via intermittant current pulses is receiving growing attention as an alternative to constant (direct) current electroplating. An expanding list of metal plating systems shows pulse electrolysis process advantages over conventional d.c. electrodeposition. These advantages are essentially of two types.

1. Improvements in the local deposit properties, e.g. film density and alloy composition (for the case of alloy plating).
2. Better control of film deposition rates across macroscopic dimensions of the substrate, generally with emphasis on film thickness or resistance uniformity in systems with poorly conducting substrates and/or non-uniform ionic solution resistance distributions between anode and cathode.

Improvements of type 1 have been observed for many metals of electroplating interest and are reviewed elsewhere [1–11]. Moreover, supporting theoretical analyses, derived on the basis of mass transport models developed by Ibl *et al.* [9, 12] and Cheh *et al.* [13–15], provide useful insights into the origin of microscopic field property differences between d.c. and pulse current electrodeposition.

There is, by contrast, no model to explain the deposit thickness 'levelling' behaviour observed with pulse current electroplating. Although plating thickness levelling can, in principle, be ascribed to cell operation under limiting mass transport control with single-step kinetics, the resulting microscopic plate characteristics are generally unacceptable. To achieve limiting mass transport current conditions over a poorly conducting electrode with peripheral electrical contact, for example, a large potential difference will develop across the substrate, promoting significant coproduction of hydrogen in the vicinity of the electrode contact. The inability to predict levelling behaviour at area-averaged current densities, i_{avg}, far below the mass transport limiting current density, i_{lim}, represents a second major shortcoming of limiting mass transfer models.

0021–891X/86 $03.00 + .12

Ibl [9] and more recently Cheh [17] have addressed the role of non-Faradaic (electrical double layer) capacitance on pulse current electrodeposition. Here, too, the derived models are incapable of accounting for the observed deposit levelling behaviour.

Remarkably, despite growing interest in pulse current processes, published pulse current electroplating theories have not evolved beyond treatments of simple, single-step reaction kinetics. In particular there has been no account of Faradaic capacitances arising from multiple-step electrode kinetics. The omission of this phenomenon is responsible for the inability to mechanistically interpret observed current density levelling effects. Indeed, the levelling behaviour can be readily predicted at $i_{avg} \ll i_{lim}$ by accounting for multiple-step kinetics and associated Faradaic pseudocapacitances, as shown below.

2. Current distribution analysis

Consider the case of a poorly conducting circular disc with an electrical contact at the other disc edge, operated transiently as the cathode in a cylindrically symmetrical cell. Via symmetry arguments, the transient total and Faradaic current density distributions, $i_T(r, t)$ and $i_F(r, t)$, need to be analysed at only a single, arbitrary cylindrical angle, θ_0, reducing the analysis to a question of current density along a line, L, containing all points (r, θ_0) between $(0, \theta_0)$ and (R, θ_0).

Fig. 1 shows the distributed component representation of the current pathway between the cathode contact and the potential null point between anode and cathode. The latter is defined as the axial position, y, for which the potential in a cylindrically symmetrical cell is constant, with variations in radial and angular position (r, θ). Here k represents the kth line element, covering the range $k = 1$ $(r = R)$ to $k = n$ $(r = 0)$. Note that Fig. 1 does not require invariance of solution resistance, R_S, with radial position. However, in order to clarify the mechanism of thickness levelling on a poorly conducting substrate, all $R_S(k)$ will be assumed negligible in comparison to corresponding electronic resistances within the electrode, $R_E(k)$.

The appearance of two capacitance components for every line element is a central feature of the ladder network shown in Fig. 1. The electrical double-layer capacitance is given by C_{DL}. To simplify the discussion which follows, the electrical double-layer capacitance is taken as a constant, thus implicitly assuming a high ionic strength.

The second capacitance, C_P, is the (Faradaic) pseudocapacitance. Most simply, the pseudocapacitance represents the ability to store charge by altering the coverage of adsorbed reaction intermediates. As a reaction term, the pseudocapacitance is a strong function of electrode potential, $\phi(r, t)$, and interfacial reactant and product concentrations. To make this discussion more specific, the plating reaction mechanism will be taken to follow Reactions 1–4

$$M^{m+} + e \rightarrow M^{(m-1)+} \quad (1)$$

$$M^{(m-1)+} + e \rightarrow M^{(m-2)+} \quad (2)$$

$$\vdots$$

$$M^{+} + e \rightarrow M_{ads} \quad (3)$$

$$M_{ads} \rightarrow M \quad (4)$$

where, under steady state conditions, the final step is rate controlling. The interfacial resistance, R_F, thus represents the ability to pass charge via Reaction 4. The net reaction rate, v, for Reaction 4 can be simply written as

$$v = K(\theta - \theta_e) \quad (5)$$

where θ and θ_e are the instantaneous and equilibrium fractional surface converges of absorbed M.

The total impedance at the cathode contact, $Z(R, t)$, can be most readily formulated in terms of

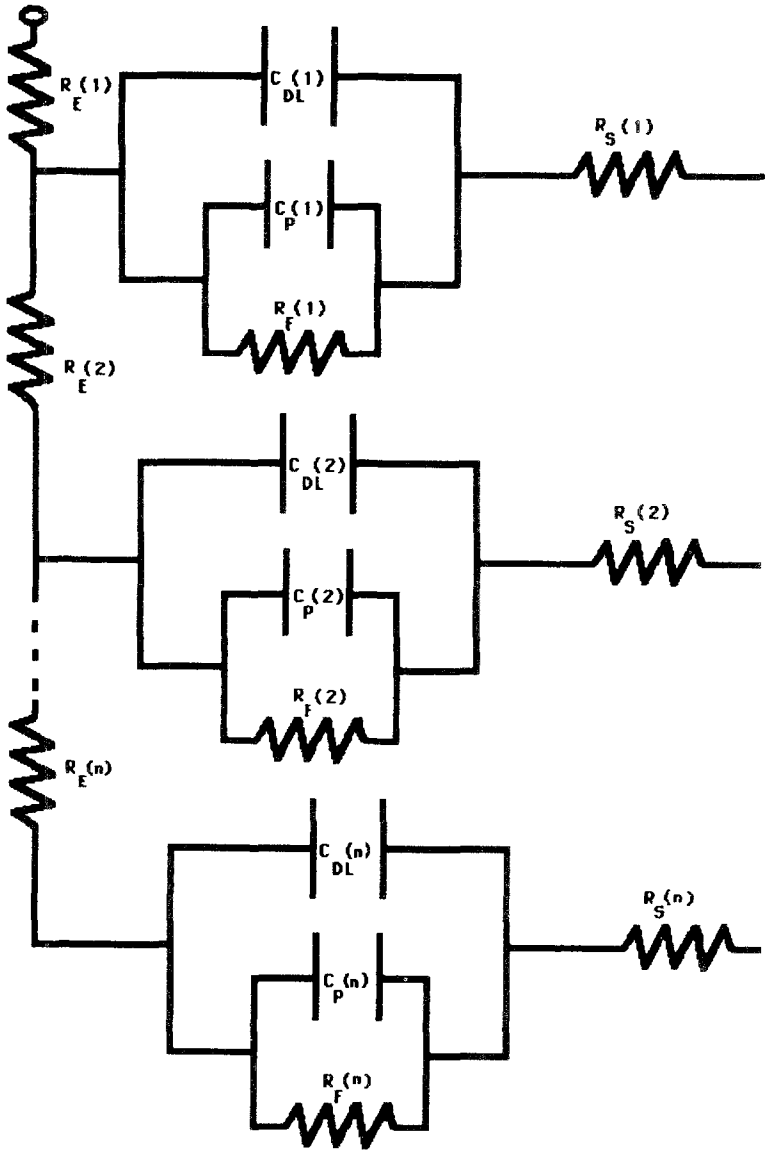

Fig. 1. Distributed component network representation, cathode contact to the potential null point.

its associated transfer function $z(R, S)$. The latter is simply the Laplace transform of $Z(R, t)$: $z(R, S) = \mathscr{L}(Z(R, t))$. Moreover, by direct application of nonlinear network analysis methods $z(R, S)$ reduces to a continued fraction. Thus the term for the ℓth element is

$$z(r_\ell, S) = R_E(\ell) + \cfrac{1}{y(\ell) + \cfrac{1}{R_E(\ell+1) + \cfrac{1}{y(\ell+1) + \cfrac{1}{\ddots \\ \vdots \\ R_E(n) + \cfrac{1}{y(n)}}}}} \tag{6}$$

Here the component value $y(\ell)$ represents the transformed admittance of the ℓth shunt arm, with

$$y(\ell) = (C_{DL} + C_P(\ell))\left[S + \frac{1}{(C_{DL} + C_P(\ell))R_F(\ell)}\right] \quad (7)$$

The variation of $i_F(r, t)$ over the spatial range $0 \leqslant r \leqslant R$ is determined by the relative variation of what can be termed the 'total and Faradaic pathway impedance' over the full range of radial positions. Both impedance characteristics are important; the former controls the potential distribution, which, together with the Faradaic impedance, dictates the transient Faradaic current density distribution.

3. Approximate analysis

Full analysis of the problem briefly posed here, although conceptually straightforward, is mathematically complex, generally requiring recourse to digital computation [18]. Two additional problems are associated with the full solution approach. First, as mentioned above, the large number of system and control variables make it difficult to determine systematically parameter influences, such as general scaling laws or routines for determining optimum parameter values. The second problem involves uncertainties in the quantitative relationship for the Faradaic pseudocapacitance, posing a serious difficulty for analyses performed over a broad range of system conditions.

In recognition of the difficulties inherent in obtaining a general yet exact solution, it is viewed appropriate to demonstate an approximate analysis technique for the system case displaying the greatest benefit from pulse current operation. Therefore, the following limiting behaviour is assumed:

(a) poorly conducting substrate,
(b) large reaction pseudocapacitance maximum relative to C_{DL},
(c) Reaction 4 is rate-controlling,
(d) no influences from primary current distribution effects in the electrolyte, i.e. all $R_S(k)$ can be neglected,
(e) C_{DL} is constant.

The primary point in this semiquantitative analysis is recognition that θ tends to a saturation value (unity) with increasing negative potential, and C_P displays a strong potential dependence, regardless of the adsorption isotherm details. Most importantly, C_P varies from a value more than an order of magnitude greater than C_{DL} (at intermediate θ), to values much smaller than C_{DL} at $\theta \cong 1$.

These comments clearly suggest the mechanism of current levelling. At any position r, current can pass the electrode/electrolyte interface by one of the three component mechanisms outlined in Fig. 2:

(a) charging of the electrical double layer,
(b) charging of the Faradaic reaction intermediate inventory,
(c) passage of Faradaic current without alteration of θ.

For the limiting conditions assumed here, in particular a very slow Reaction 4, only mechanisms (a) and (b) are capable of supporting large interfacial current densities (though only on a transient basis). Beginning with the system at equilibrium and then suddenly passing an electrode current, I_A, the responding interfacial current density will be distributed across the electrode as a moving front beginning at $r = R$, due to the more negative potential and associated larger C_P at this position at early times ($t \ll t_A$). With continuing passage of current, $\theta(R) \sim 1$ and $C_P(R)$ correspondingly drops. The maximum in interfacial current density moves to smaller values of r, leaving behind a saturated surface.

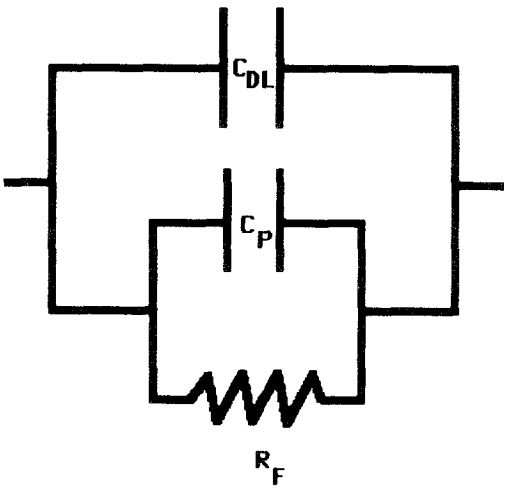

Fig. 2. Component representation of local interfacial impedance.

Consider the time, t_A, required to achieve $\theta(0) = 0.999$. During this time, Reaction 4 has been proceeding in region $l = 1$ ($r = R$) via a rate given by Equation 5, with $\theta \cong 1$, i.e. at a rate $v(R) = K(1 - \theta)$. The ratio of excess reaction at element 1 to the adsorbed reactant at the nth element ($r = 0$) is given by ψ_A:

$$\psi_A = \frac{v(R)t_A}{\Gamma[\theta(0) - \theta_e)]} = \frac{K(1 - \theta_e)t_A}{\Gamma(0.999 - \theta_e)} \sim \frac{Kt_A}{\Gamma} \tag{8}$$

Here Γ is the surface charge density associated with adsorption of a monolayer coverage, $\theta = 1$.

During the zero current period, the charge stored in the electrical double layer will discharge by driving Reaction 4

$$-nFK(1 - \theta_e) = C_{DL}\frac{d\phi}{dt} \tag{9}$$

When sufficient electrical double layer charge has been discharged, the local electrode potential will drop to values yielding $C_P \sim C_{DL}$ and the contribution of pseudocapacitance must be accounted for:

$$\frac{d(C_P\Delta\phi)}{dt} - nFK(\theta - \theta_e) = C_{DL}\frac{d\phi}{dt} \tag{10}$$

At this stage, e.g. for $\theta < 0.999$, the plating behaviour at all elements is essentially identical, with negligible contribution to plate thickness variations with r.

Between the off-time, t_B, corresponding to $\theta(R) = 1.000$ and $\theta(R) = 0.999$, however, the discharge process represented by Equation 9 will produce an excess charge at the outer element given by $C_{DL}[\phi(R, t_A) - \phi(0, t_A)]$. The ratio of excess plating reaction at element 1 produced by this discharge process, to the pseudocapacitatively stored charge at the nth element is given by ψ_B:

$$\psi_B = C_{DL}\frac{[\phi(R, t_A) - \phi(0, t_A)]}{\Gamma(0.999 - \theta_e)} \tag{11}$$

Evaluation of Equation 11 is primarily an issue of determining $[\phi(R, t_A) - \phi(0, t_A)]$. This potential difference is computable by the network analysis technique outlined above. A characteristic of this analysis is the observation that the electrode current distribution, $I(r)$, can be expressed as a polynomial series.

$$I(r) = I_A\frac{\left[\alpha_0 + \alpha_1\left(\frac{r}{R}\right) + \alpha_2\left(\frac{r}{R}\right)^2 + \alpha_3\left(\frac{r}{R}\right)^3 + \ldots + \alpha_g\left(\frac{r}{R}\right)^g\right]}{(\alpha_0 + \alpha_1 + \alpha_2 + \alpha_3 + \ldots + \alpha_g)} \tag{12}$$

The polynomial coefficients a_j are determined by the full network analysis. The radial potential gradient $d\phi/dr$ is related to the local intra-electrode current, $I(r)$, via

$$\frac{d\phi}{dr} = \frac{I(r)}{2\pi rh\kappa} \tag{13}$$

where h and κ are the electrode thickness and electronic conductivity, respectively. Substituting Equation 13 into Equation 12 and integrating Equation 17 over the limits $r = R$ to $r = 0$

$$\phi(R, t) - \phi(0, t) = (2\pi h\kappa f)^{-1} f' I_A \tag{14}$$

where $f = (\alpha_0 + \alpha_1 + \alpha_2 + \alpha_3 + \ldots + \alpha_g)$
and $f' = \alpha_1 + \alpha_2/2 + \alpha_3/3 + \ldots \alpha_g/g$
It is important to note that under the conditions specified here, i.e. t_A chosen to be sufficiently long to achieve $\theta(0, t_A) = 0.999$, the interfacial impedance at early stages of period B is controlled by the electrical double-layer capacitance and steady-state Faradaic resistance (with $\theta \sim 1$). Thus, the current distribution given in Equation 12 can be evaluated without including reaction pseudo-capacitance terms. This greatly simplifies the analysis task, for under these saturation conditions ($\theta \sim 1$) both R_F and C_{DL} are independent of I_A for $i_{avg} \ll i_{lim}$. Via similar arguments, all α_j are also independent of I_A within this current density range. Note, however, that because of the distributed relaxation timescales, α_j are functions of t_A.

For a specific choice of t_A, Equations 12 and 14 may be combined, giving

$$\psi_B = \frac{C_{DL} f' I_A}{2\pi h\kappa f \Gamma(0.999 - \theta_e)} \tag{15}$$

The most characteristic single measure of current maldistribution is the extreme cycle value, ψ,

$$\psi = \psi_A + \psi_B \tag{16}$$

Before final evaluation of Equation 16 can be made, the value of t_A must be given. On the basis of a charge balance

$$t_A = [\pi R^2 \Gamma(1 - \theta_e) + \Delta Q_{DL}] I_A^{-1} \tag{17}$$

Here ΔQ_{DL} is the charge stored in the electrical double-layer, relative to the double-layer charge which would be stored if the entire electrode potential were held at $\phi(0, t_A)$:

$$\Delta Q_{DL} = \frac{C_{DL} I_A R^2 f''}{h\kappa f} \tag{18}$$

with

$$f'' = \frac{\alpha_1}{3} + \frac{\alpha_2}{8} + \ldots + \frac{\alpha_g}{g(g + 2)}$$

Combining Equations 8, 15 and 18 in Equation 16

$$\psi = \left(\pi R^2 \Gamma(1 - \theta) + \frac{C_{DL} I_A R^2 f''}{h\kappa f}\right) K\Gamma^{-1} I_A^{-1} + \frac{C_{DL} f' I_A}{2\pi h\kappa f \Gamma(0.999 - \theta_e)} \tag{19}$$

4. Optimization

Taking the first derivative of ψ with respect to on-time current

$$\frac{d\psi}{dI_A} = -\pi R^2 \Gamma(1 - \theta_e) I_A^{-2} \frac{K}{\Gamma} + \frac{C_{DL} f'}{2\pi h\kappa f \Gamma(0.999 - \theta_e)} \tag{20}$$

The corresponding optimum on-time current is thus

$$I_{A_{opt}} = \pi R \left[\frac{2h\kappa K\Gamma f(0.999 - \theta_e)}{C_{DL} f'}\right]^{1/2} \tag{21}$$

The optimum on-time period is obtained upon combining Equations 17, 18 and 21:

$$t_{A_{opt}} = \frac{R(1 - \theta_e)}{\left[\frac{2h\kappa Kf}{\Gamma C_{DL} f'}(0.999 - \theta_e)\right]^{1/2}} + \frac{C_{DL} R^2 f''}{h\kappa f} \tag{22}$$

This expression is mathematically more cumbersome than the relation for $I_{A_{opt}}$. Specifically, the dependence of α_j on t_A gives Equation 22 a transcendental character. Substitution of $I_{A_{opt}}$ into Equation 19 yields ψ_{min}, the minimum extreme thickness variation.

A key feature of the functional form displayed in Equation 23 is the relative insensitivity of ψ on I_A for currents within a considerable current value range around $I_{A_{opt}}$. The origin of this weak current dependence is, of course, the offsetting current functionalities of ψ_A and ψ_B. For typical system parameters, ψ varies by no more than 5% for $0.7 < I_A/I_{A_{opt}} < 1.3$, and by less than 40% for $0.5 < I_A/I_{A_{opt}} < 2.0$. Such results are in substantial agreement with experimental observations which show a weak dependence of thickness levelling behaviour on total electrode current within a relatively wide current range.

5. Discussion

The semi-quantitative results (Equations 21 and 22) demonstrate that for a particular system choice there exists an optimum on-time current and an optimum on-time period. The obtained functional dependence of $I_{A_{opt}}$ and $t_{A_{opt}}$ on system variables represents a powerful resource for pulse current system analysis, including scaling. On the latter point, Equation 22 demonstrates that for the limiting case (α_j independent of R), $I_{A_{opt}}$ is proportional to the disc radius. The optimum area averaged current density, $I_{A_{opt}}/\pi R^2$, therefore decreases with increasing R, reducing the rate at which pulse current plating can be performed on larger substrates. However, because of the mixed R dependencies of ψ, the ability to achieve a specific degree of thickness levelling with variations in R is strongly dependent on system parameters, with possible ψ_{min} vs R dependencies ranging for R^{-1} to R^2.

The choice of optimum off-current period length is influenced by two conflicting trends. Levelling performance improves with increasing t_B, at the expense of duty cycle. On the basis of relaxation timescales, the minimum practical value of t_B is $t_{B_{min}} \gg (t_{A_{opt}} \langle C_P \rangle / C_{DL}) \sim t_{A_{opt}} C_{P_{max}} / C_{DL}$, where $\langle C_P \rangle$ and $C_{P_{max}}$ are the pulse averaged and maximum pseudocapacitances, respectively. Typically this yields t_B/t_A of order ten, in substantial agreement with optimum off-to-on time period ratios for thickness levelling.

References

[1] G. W. Jernstedt, *Ann. Proc. Amer. Electroplaters' Soc.* **36** (1949) 63.
[2] A. J. Avila and M. J. Brown, *Plating* **57** (1970) 1105.
[3] A. R. Despic and K. I. Popov, *J. Appl. Electrochem.* **1** (1971) 275.
[4] C. C. Wan, H. Y. Cheh and H. B. Linford, *Plating* **61**(1974) 559.
[5] W. Sullivan, *ibid.* **62** (1975) 139.
[6] J. D. E. McIntyre and W. F. Peck, Jr., *J. Electrochem. Soc.* **123** (1976) 1800.
[7] Ch. J. Raub and A. Knodler, *Gold Bull.* **10** (1977) 38.
[8] L. Missel and T. Montelbano, *Electron. Packag.*, April, (1978) 166.
[9] N. Ibl, *Surf. Technol.* **10** (1980) 81.
[10] L. Missel, P. Duke, and T. Montelbano, *Semiconductor Int.*, February 67 (1980).
[11] N. Ibl, *J. Electrochem. Soc.* **114** (1967) 1268.
[12] N. Ibl, J. C. Puippe and H. Angerer, *Surf. Technol.* **6** (1978) 287.
[13] H. Y. Cheh, *J. Electrochem. Soc.* **118** (1971) 551.
[14] K. Viswanathan, M. A. Farrell Epstein, and H. Y. Cheh, *ibid.* **125** (1978) 1772.
[15] K. Viswanathan and H. Y. Cheh, *ibid.* **125** (1978) 1616.
[16] K. Viswanathan, H. Y. Cheh and G. L. Standart, *J. Appl. Electrochem.* **10** (1980) 37.
[17] H. Y. Cheh, International Society of Electrochemistry, 35th Meeting, Abstract B6-6.
[18] H. E. Hager, in preparation for *J. Appl. Electrochem.*